

# Proton decay matrix elements on the lattice

Y. Aoki,<sup>1,2,\*</sup> E. Shintani,<sup>2,†</sup> and A. Soni<sup>3,‡</sup>

(RBC and UKQCD collaborations)

<sup>1</sup> *Kobayashi-Maskawa Institute for the Origin of Particles and the Universe (KMI),*

*Nagoya University, Nagoya 464-8602, Japan*

<sup>2</sup> *RIKEN-BNL Research Center, Brookhaven National Laboratory, Upton, NY 11973, USA*

<sup>3</sup> *High Energy Theory Group, Brookhaven National Laboratory, Upton, NY 11973, USA*

## Abstract

Hadronic matrix elements of proton decay are essential ingredients to bridge the grand unification theory to low energy observables like proton lifetime. In this paper we non-perturbatively calculate the matrix elements, relevant for the process of a nucleon decaying into a pseudoscalar meson and an anti-lepton through generic baryon number violating four-fermi operators. Lattice QCD with 2+1 flavor dynamical domain-wall fermions with the *direct* method, which is direct measurement of matrix element from three-point function without using chiral perturbation theory, are used for this study to have good control over the error due to lattice discretization effects, operator renormalization, and chiral extrapolation. The relevant form factors for possible transition process from an initial proton or neutron to a final pion or kaon induced by all types of three quark operators are obtained through three-point functions of (nucleon)-(three-quark operator)-(meson) with physical kinematics. In this study all the relevant systematic uncertainties of the form factors are taken into account for the first time, and the total error is found to be the range 30%–40% for  $\pi$  and 20%–40% for  $K$  final states.

PACS numbers: 11.15.Ha,12.38.Gc,12.10.Dm

---

\*Electronic address: yaoki@kmi.nagoya-u.ac.jp

†Electronic address: shintani@riken.jp

‡Electronic address: adlersoni@gmail.com

## I. INTRODUCTION

Proton decay is a smoking gun evidence of physics beyond the standard model and is a natural outcome of Grand Unified Theories (GUTs) [1, 2]. The process occurs through baryon number changing interactions mediated by the heavy new particles. Dominant modes are of X and Y gauge boson exchange for GUTs and of color-triplet Higgs multiplet for supersymmetric (SUSY) GUTs [3, 4]. Recent SuperKamiokande experiments report the bound on proton partial lifetime, for instance,  $\tau > 8.2 \times 10^{33}$  year for the  $p \rightarrow e^+ \pi^0$  channel [5, 6], which is typical for gauge boson exchange, or  $\tau > 2.3 \times 10^{33}$  for  $p \rightarrow K^+ \bar{\nu}$  [7] and  $\tau > 1.6 \times 10^{33}$  for  $p \rightarrow K^0 \bar{\mu}^+$  [8], both of which are favored for some SUSY GUTs. There have been many arguments of a constraint on proton lifetime from various types of GUT models so far (see a comprehensive review [9] and reference therein). In order to constrain the parameter space in GUT models with a reliable bound, a removal of all the theoretical uncertainties is highly desirable. One of the important elements, which can be made less uncertain from the current knowledge, is the hadronic contribution to proton decay matrix elements. Lattice QCD calculation can lead to reducing the uncertainties in the hadronic matrix element of a nucleon decaying into a pseudoscalar meson, and thus it can provide relevant information for the proton lifetime bound and help experimental plans for the future [10].

The estimate of proton decay matrix elements in lattice QCD has been significantly improved by removing systematic errors, one by one, since the first attempts in 1980s [11–13]. A decade ago JLQCD collaboration [14] performed an extensive calculation of proton decay matrix elements using Wilson fermion action and operator renormalization estimated by one-loop lattice perturbation in the quenched approximation with both the “*direct*” method, which is a direct measurement of matrix element from three-point functions, and the “*indirect*” method, which is an effective estimate through low-energy constants in tree-level chiral perturbation theory, calculated with two-point functions. Few years later JLQCD and CP-PACS joint collaboration carried out a continuum extrapolation of the low energy constants for the *indirect* method [15] to control the uncertainty of large discretization error. Using the *direct* method, RBC collaboration [16] performed the analysis with quenched domain-wall fermions (DWFs) and non-perturbative renormalization, where thanks to almost exact chiral symmetry of the DWFs the discretization error of  $\mathcal{O}(a)$  is essentially removed and

the error of renormalization factor associated with the use of lattice perturbation theory was also eliminated. The RBC collaboration also performed the DWF calculation using the *indirect* method with quenched approximation as well as with unquenching  $u$  and  $d$  quarks [16], and later the RBC and UKQCD collaborations extended the DWF calculation of the *indirect* method using three dynamical quarks ( $u$ ,  $d$  and  $s$ ) [17]. In this way, one of the uncontrolled systematic uncertainty coming from quenched approximation was removed.

A striking, but perhaps not surprising outcome of the comparison of the results from *direct* and *indirect* calculations, though performed only with quenched approximation so far, is that the *indirect* method could overestimate the matrix elements by a factor of about two [16]. To fully control the systematic uncertainties, therefore, one needs to perform the *direct* calculation with the  $N_f = 2 + 1$  dynamical simulations and a non-perturbative operator renormalization.

In this paper we provide the non-perturbative estimate of proton decay matrix elements using the *direct* method with the dynamical,  $N_f = 2 + 1$  (degenerate  $u$ ,  $d$  and physical  $s$  quarks) flavor lattice QCD with DWFs. The DWF ensemble for  $N_f = 2 + 1$  at the lattice cutoff  $a^{-1} \sim 1.7$  GeV with 300–700 MeV pion masses [18] in RBC/UKQCD collaboration are used for this purpose, and thus this enables us to evaluate hadronic matrix elements including almost all systematic errors on the lattice.

This paper is organized as follows. In section II we explain the definition and property of the matrix elements as well as their relation to the proton partial decay width. The method to extract the matrix elements from three-point function on the lattice is expressed in section III, and in section IV we present our setup and the detailed analysis to obtain the matrix elements and evaluate their systematic uncertainties. Section V is devoted to summary and outlook.

## II. PROTON DECAY MATRIX ELEMENT

### A. Effective Lagrangian and matrix element

Baryon number violating operators appearing in the leading low-energy effective Hamiltonian are constructed by possible combination of dimension-six (three quarks and one lepton) operators to be  $SU(3)$  color singlets and  $SU_L(2) \times U_Y(1)$  invariant. Following the notation

of [19–21], four-fermi operators are expressed as

$$O_{abcd}^{(1)} = (D_a^i, U_b^j)_R (q_c^{k\alpha}, l_d^\beta)_L \varepsilon^{ijk} \varepsilon^{\alpha\beta}, \quad (1)$$

$$O_{abcd}^{(2)} = (q_a^{i\alpha}, q_b^{j\beta})_L (U_c^k, l_d)_R \varepsilon^{ijk} \varepsilon^{\alpha\beta}, \quad (2)$$

$$\tilde{O}_{abcd}^{(4)} = (q_a^{i\alpha}, q_b^{j\beta})_L (q_c^{k\gamma}, l_d^\delta)_L \varepsilon^{ijk} \varepsilon^{\alpha\delta} \varepsilon^{\beta\gamma}, \quad (3)$$

$$O_{abcd}^{(5)} = (U_a^i, D_b^j)_R (U_c^k, l_d)_R \varepsilon^{ijk}, \quad (4)$$

with generic lepton field  $l$ , and quark field of left-handed part  $q$  and right-handed part  $U$  and  $D$  as up and down type. The indices  $a, b, c, d$  denote the generation number of fermion,  $i, j, k$  denote color SU(3) indices, and  $\alpha, \beta, \gamma, \delta$  are SU(2) indices. The inner product is defined as  $(x, y)_{R/L} = x^T C P_{R/L} y$  which has charge conjugation matrix  $C$  and chiral projection  $P_{R/L}$ . The baryon number violation (but preserving  $B-L$  number) in GUT models is generally expressed as low-energy effective Hamiltonian with the above six-dimension operators. Leading term of effective Hamiltonian at low energies is represented as

$$\mathcal{L}^{\mathcal{B}} = \sum_I C^I [(qq)(ql)]^I + \dots = - \sum_I C^I [\bar{l}^c \mathcal{O}_{qqq}]^I + \dots, \quad (5)$$

where  $C^I = C^I(\mu)$  is the Wilson coefficient with renormalization scale  $\mu$  of the operator  $[(qq)(ql)]^I$  with  $q$  being a light quark flavor  $u, d$ , or  $s$ . The operator is one of those appearing in Eq.(1)–(4), and renormalized also at  $\mu$ . The details of the (SUSY) GUT is all captured in the coefficients  $C^I(\mu)$ . Ellipsis means the higher order operators which are suppressed by inverse power of heavy mass scale. The index  $I$  distinguishes the type of operator with respect to the quark-lepton flavor and chirality. The three-quark operator reads

$$\mathcal{O}_{qqq}^{\Gamma\Gamma'} = (qq)_\Gamma q_{\Gamma'} = \varepsilon^{ijk} (q^{iT} C P_\Gamma q^j) P_{\Gamma'} q^k, \quad (6)$$

where the color singlet contraction is taken. Dirac spinor indices are omitted in the above equation. In the following we may use simple notations for the three-quark operators as  $\mathcal{O}^{\Gamma\Gamma'}$ .  $\Gamma$  and  $\Gamma'$  denote the chirality, either  $R$  or  $L$  and the bracket means the contractions among Dirac spinors.

We calculate the transition matrix elements of the dimension-six operators with an initial nucleon (proton or neutron,  $N = p, n$ ) state and a final state containing a pseudoscalar meson ( $P = (\pi, K, \eta)$ ) and an anti-lepton ( $\bar{l}$ )

$$\langle P(\vec{p}), l(\vec{q}, s) | [\bar{l}^c \mathcal{O}^{\Gamma\Gamma'}] | N(\vec{k}) \rangle = \bar{v}_l^c(q, s) \langle P(\vec{p}) | \mathcal{O}^{\Gamma\Gamma'} | N(\vec{k}, s) \rangle, \quad (7)$$

including three-dimensional momenta,  $\vec{p}$  for final pseudoscalar,  $\vec{k}$  for initial nucleon and  $\vec{q} = \vec{p} - \vec{k}$  for final lepton which is determined from momentum conservation. Neglecting the electroweak interaction of the lepton, the amplitude  $\langle l(\vec{q}, s) | \bar{l}^c | 0 \rangle = \bar{v}_l^c(\vec{q}, s)$  of the lepton part can be captured in the wave function of on-shell lepton state at momentum  $\vec{q}$  for spin  $s$  component. The matrix element  $\langle P(\vec{p}) | \mathcal{O}^{\Gamma\Gamma'} | N(\vec{k}, s) \rangle$  is parametrized by the relevant form factor  $W_0(q^2)$  and irrelevant one  $W_1(q^2)$  as

$$\langle P(\vec{p}) | \mathcal{O}^{\Gamma\Gamma'} | N(\vec{k}, s) \rangle = P_{\Gamma'} \left[ W_0^{\Gamma\Gamma'}(q^2) - \frac{i\not{q}}{m_N} W_1^{\Gamma\Gamma'}(q^2) \right] u_N(k, s). \quad (8)$$

$W_0$  and  $W_1$  are defined for each matrix element with the three-quark operator renormalized in  $\overline{MS}$  NDR at scale  $\mu$ , and are functions of square of four momentum transfer  $q = k - p$ . Using on-shell condition, the total matrix element as shown in Eq.(7) is given by

$$\begin{aligned} \bar{v}_l^c(q, s) \langle P(\vec{p}) | \mathcal{O}^{\Gamma\Gamma'} | N(\vec{k}, s) \rangle &= \bar{v}_l^c(q, s) P_{\Gamma'} \left[ W_0^{\Gamma\Gamma'}(q^2) - \frac{i\not{q}}{m_N} W_1^{\Gamma\Gamma'}(q^2) \right] u_N(k, s) \\ &= \bar{v}_l^c(\vec{q}, s) P_{\Gamma'} u_N(\vec{k}, s) W_0^{\Gamma\Gamma'}(0) + O(m_l/m_N), \end{aligned} \quad (9)$$

with  $i\not{q}v_l = m_l v_l$  and  $W_1 \simeq W_0$  [16]. Since  $-q^2 = m_l^2$  is much smaller than nucleon mass squared in the case of  $l = e, \nu$ , we set  $q^2 = 0$  and ignore the second term in Eq.(9). Taking only the relevant form factor will be a good approximation even for  $l = \mu$ , as  $m_\mu/m_N \sim 10\%$  is smaller than the total error of  $W_0$  in this study.

Once the relevant form factor  $W_0$  is obtained in lattice QCD, the partial decay width of the decay  $N \rightarrow P + \bar{l}$  is given by

$$\Gamma(N \rightarrow P + \bar{l}) = \frac{m_N}{32\pi} \left[ 1 - \left( \frac{m_P}{m_N} \right)^2 \right]^2 \left| \sum_I C^I W_0^I(N \rightarrow P) \right|^2 \quad (10)$$

with the perturbative estimate of Wilson coefficient  $C^I$  in the GUT models [9]. Note that renormalization scale dependence of  $C^I$  and  $W_0^I$  cancels out in their multiplication.

The different chirality combinations of the matrix elements are related through the Parity transformation as

$$\langle P; \vec{p} | \mathcal{O}^{RL} | N; \vec{k}, s \rangle = \gamma_0 \langle P; -\vec{p} | \mathcal{O}^{LR} | N; -\vec{k}, s \rangle, \quad (11)$$

$$\langle P; \vec{p} | \mathcal{O}^{LL} | N; \vec{k}, s \rangle = \gamma_0 \langle P; -\vec{p} | \mathcal{O}^{RR} | N; -\vec{k}, s \rangle, \quad (12)$$

which indicates that four chirality combinations  $(\Gamma\Gamma') = (RL), (LL), (LR), (RR)$  are reduced to two different combinations,  $(\Gamma\Gamma') = (RL), (LL)$ . In the following  $\Gamma'$  is fixed in

a left-handed chirality, and a short-hand notation  $W_{0,1}^{\Gamma L} \equiv W_{0,1}^{\Gamma}$  is used. Under exchange-symmetry between  $u$  and  $d$  there are the following relations between proton and neutron matrix elements:

$$\langle \pi^0 | (ud)_{\Gamma} u_L | p \rangle = \langle \pi^0 | (du)_{\Gamma} d_L | n \rangle, \quad (13)$$

$$\langle \pi^+ | (ud)_{\Gamma} d_L | p \rangle = -\langle \pi^- | (du)_{\Gamma} u_L | n \rangle, \quad (14)$$

$$\langle K^0 | (us)_{\Gamma} u_L | p \rangle = -\langle K^+ | (ds)_{\Gamma} d_L | n \rangle, \quad (15)$$

$$\langle K^+ | (us)_{\Gamma} d_L | p \rangle = -\langle K^0 | (ds)_{\Gamma} u_L | n \rangle, \quad (16)$$

$$\langle K^+ | (ud)_{\Gamma} s_L | p \rangle = -\langle K^0 | (du)_{\Gamma} s_L | n \rangle, \quad (17)$$

$$\langle K^+ | (ds)_{\Gamma} u_L | p \rangle = -\langle K^0 | (us)_{\Gamma} d_L | n \rangle, \quad (18)$$

$$\langle \eta | (ud)_{\Gamma} u_L | p \rangle = -\langle \eta | (du)_{\Gamma} d_L | n \rangle. \quad (19)$$

A negative sign comes from the interpolation operator of proton or neutral pion by the exchange of  $u$  and  $d$ . Furthermore in the SU(2) isospin limit there is an additional relation between Eq.(13) and Eq.(14):

$$\langle \pi^0 | (ud)_{\Gamma} u_L | p \rangle = \sqrt{2} \langle \pi^+ | (ud)_{\Gamma} d_L | p \rangle. \quad (20)$$

Therefore there are twelve principal matrix elements we calculate in this paper.

### III. CALCULATION SCHEME FOR THE FORM FACTORS

To obtain the matrix element we make use of the ratio of three-point function of (proton)-( $O^{\Gamma L}$ )-(meson) and two-point function of nucleon and meson. Such a ratio is represented as

$$\begin{aligned} & R_3(t, t_1, t_0; \vec{p}, \mathcal{P}) \\ &= \frac{\sum_{\vec{x}, \vec{x}_1} e^{i\vec{p}(\vec{x}_1 - \vec{x})} \text{tr} [\mathcal{P} \langle 0 | J_P^{\text{gs}}(\vec{x}_1, t_1) \mathcal{O}^{\Gamma L}(\vec{x}, t) \bar{J}_p^{\text{gs}}(\vec{0}, t_0) | 0 \rangle]}{\sum_{\vec{x}, \vec{x}_1} e^{i\vec{p}(\vec{x}_1 - \vec{x})} \langle 0 | J_P^{\text{gs}}(\vec{x}_1, t_1) J_P^{\text{gs}\dagger}(\vec{x}, t) | 0 \rangle \sum_{\vec{x}} \text{tr} [P_4 \langle 0 | J_p^{\text{gs}}(\vec{x}, t) \bar{J}_p^{\text{gs}}(\vec{0}, t_0) | 0 \rangle]} \sqrt{Z_P^{\text{gs}}(\vec{p}) Z_p^{\text{gs}} L_\sigma^3}, \end{aligned} \quad (21)$$

with interpolating field for pseudoscalar  $J_P^{\text{gs}}$  and proton  $J_p^{\text{gs}}$ . These interpolating operators are made of quark fields smeared using the gauge-invariant Gaussian smearing [22] with the parameters optimized for meson and proton separately. In the periodic lattice the injected spatial momentum is  $\vec{p} = 2\pi\vec{n}/L_\sigma$ , where  $\vec{n}$  is integer vector  $0 \leq n_i \leq L_\sigma - 1$ , and  $L_\sigma$

is the spatial extension of the lattice. “tr” represents trace over spinor indices, and  $\mathcal{P}$  is a spin projection matrix. The three-point function in numerator is constructed by quark propagator with the sequential source method at pseudoscalar sink location.

$Z_{P,p}$  indicates the amplitude of overlap of the interpolating field to on-shell state,

$$\langle P(\vec{p}) | J_P^{\text{gs}\dagger}(0) | 0 \rangle = \sqrt{Z_P^{\text{gs}}(\vec{p})}, \quad (22)$$

$$\langle 0 | J_p^{\text{gs}}(0) | p(\vec{0}, s) \rangle = \sqrt{Z_p^{\text{gs}}} u_p(k, s), \quad (23)$$

with the proton Dirac spinor normalized as  $\bar{u}_p(k, s)u_p(k, s') = 2m_N\delta_{ss'}$ . In this study we always take the proton to be at rest. Note that the operator of nucleon interpolating field is not uniquely determined, and we make use of the two possible proton operators formed as

$$J_p = \varepsilon^{ijk}(u^{iT}C\gamma_5d^j)u^k, \quad \varepsilon^{ijk}(u^{iT}C\gamma_4\gamma_5d^j)u^k. \quad (24)$$

Numerical comparison between the above two types of nucleon interpolating operator will be shown in the next section.

In the simulation we take the sufficiently large separation between  $t_0$  and  $t_1$  in Eq.(21) so we have a range of  $t$  where the three and two point functions in the ratio are dominated by the ground states. Then the ratio leads to its asymptotic form,

$$\lim_{t_1-t, t-t_0 \rightarrow \infty} R_3(t, t_1, t_0; \vec{p}, \mathcal{P}) = R_3^{\text{asym}}(\vec{p}, \mathcal{P}) = \text{tr} \left[ \mathcal{P} P_L (W_0^\Gamma(q^2) - \frac{i\not{q}}{m_N} W_1^\Gamma(q^2)) \right], \quad (25)$$

where  $q^2$  is the squared momentum transfer from the initial proton to the final pseudoscalar meson state  $q^2 = (k - p)^2$ . We employ two different projection matrices  $\mathcal{P} = P_4$  or  $iP_4\gamma_j$  with  $P_4 = (1 + \gamma_4)/2$  to subtract the contribution from the parity partner of the proton and to disentangle  $W_0$  and  $W_1$ . By solving the linear equations,

$$R_3^{\text{asym}}(p, P_4) = W_0^\Gamma(q^2) - \frac{iq_4}{m_N} W_1^\Gamma(q^2), \quad (26)$$

$$R_3^{\text{asym}}(p, iP_4\gamma_j) = \frac{q_j}{m_N} W_1^\Gamma(q^2). \quad (27)$$

the relevant form factor  $W_0$  can be obtained.

## IV. NUMERICAL CALCULATION OF THE PROTON DECAY FORM FACTORS

### A. Lattice setup

We use the gauge configurations generated for 2+1 flavor dynamical domain-wall fermions with Iwasaki gauge action by RBC and UKQCD collaborations [18]. The lattice volume

is  $24^3 \times 64$  and the size of the fifth dimension is  $L_s = 16$ . The gauge coupling  $\beta = 2.13$  corresponds to  $a^{-1} = 1.73(3)$  GeV. This is the same ensemble as the previous *indirect* method study [17]. Boundary condition is periodic for the gauge field, and spatially periodic and temporally anti-periodic for the fermion fields. We use four different unitary  $u$ ,  $d$  quark masses for chiral extrapolation, and one unitary and one partially quenched strange-quark mass for the study of strange quark mass dependence for final  $K^{0,+}$  kaon state. For later convenience let us introduce the quark mass  $\tilde{m}$  which includes the additive renormalization due to the inexact chiral symmetry of the domain-wall fermions at a finite extent of the fifth dimension. We define

$$\tilde{m} = m + m_{\text{res}}, \quad (28)$$

as the multiplicatively renormalizable mass with  $m$  in the lattice action, where residual mass  $m_{\text{res}}$  for the lattice used in this study has been calculated as  $m_{\text{res}} = 0.003152(43)$  [18]. The form factors of the nucleon to pion matrix elements depend on  $\tilde{m}_{ud}$  for the degenerate  $u$  and  $d$  quark mass and the squared momentum transfer  $q^2$ . For the nucleon to kaon matrix elements, the strange quark mass  $\tilde{m}_s$  enters as an additional parameter.

In the computation of the two-point and three-point function on the lattice, we employ a gauge-invariant Gaussian smearing with the optimized parameter  $(n_G, \sigma) = (40, 5.0)$  for baryon source/sink and  $(n_G, \sigma) = (16, 3.0)$  for meson sink, where the APE-smearred gauge links with  $(N, c) = (12, 0.4)$  as defined in [23]. The time slices for the nucleon source  $t_0$  and meson sink  $t_1$  are set as  $(t_0, t_1) = (5, 37)$  or  $(27, 59)$ . The baryon number violating operator at time  $t$  moves between them ( $t_0 < t < t_1$ ). We use first and second smallest but non-zero momentum  $p = (\pi/12, 0, 0)$ ,  $(\pi/12, \pi/12, 0)$  on the periodic lattice for the meson. The statistics used for each ensemble is summarized in Table I, as well as with the used valence masses and the measured  $q^2$ . Measurements are done with each 40 HMC trajectories for the ensembles with  $m_{ud} = 0.005$  and  $0.01$ , or 20 HMC trajectories for  $m_{ud} = 0.02$  and  $0.03$ . We alternate the source time slice  $t_0=5$  and  $27$  from the one to the next configuration for  $m_{ud} = 0.01, 0.02$  and  $0.03$ , while we measure both  $t_0=5$  and  $27$  for all configurations at  $m_{ud} = 0.005$  (therefore the number of measurements is doubled the number of configurations).

The multiplicative renormalization factors to convert the lattice three-quark operators in Eq.(13)–(19) into those in  $\overline{MS}$  NDR scheme has been calculated through the RI/MOM



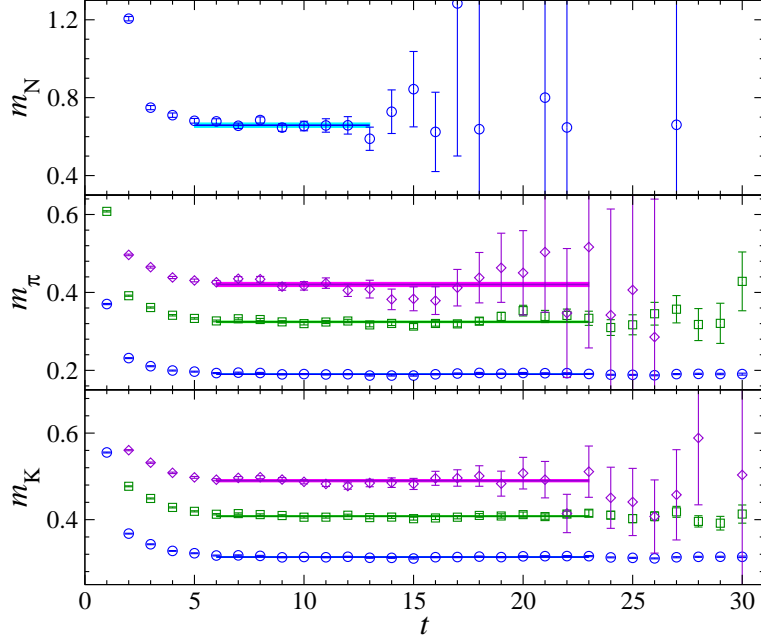


FIG. 1: Effective mass plot of nucleon (top), pion (middle) and Kaon (bottom) at momentum square  $n_p^2 = 0$  (circle),  $n_p^2 = 1$  (square),  $n_p^2 = 2$  (diamond) which correspond to  $\vec{p} = (0, 0, 0), (\pi/12, 0, 0), (\pi/12, \pi/12, 0)$  respectively. For nucleon we use gauge-invariant Gaussian source/sink, and for meson we use (Kuramashi-)wall source and gauge-invariant Gaussian sink. This is for the lightest quark mass  $m_{ud} = 0.005$  and  $m_s = 0.0343$ . Solid line (colored band) indicate the central value (statistical error) obtained by fitting.

non-perturbative renormalization [17] as

$$U(\mu = 2\text{GeV})_{LL} = 0.662(10)(53), \quad (29)$$

$$U(\mu = 2\text{GeV})_{RL} = 0.665(8)(53). \quad (30)$$

The first error is statistical one and the second is systematic one (systematic error of 8% is estimated in [17] as a truncation effect of the perturbative expansion).

In Figure 1 we show the effective mass of nucleon, pion and kaon two-point function which enter in the denominator of Eq.(21). The effective mass at time  $t$  is constructed with data at  $t$  and  $t + 1$ , and we can observe the plateau region whose starting point is  $t = 5$  for the nucleon and  $t = 6$  for the pseudoscalar. Therefore, the denominator of Eq.(21) is dominated by the ground states for  $t$  satisfying both  $t - t_0 \geq 5$  and  $t_1 - t \leq 6$ .

TABLE I: Lattice parameters, the estimate of the hadron masses and the squared momentum transfer from the initial state nucleon to the final state meson for each parameter set are shown. The lines with blank  $m_s^{\text{val}}$  entry show the kinematic parameters for the pion final state and nucleon mass, while those with  $m_s^{\text{val}}$  entry for the kaon final states. Two  $-q^2$  values in each line are for the two different momenta injected to the meson,  $\vec{p}^2 = (\pi/12)^2, 2(\pi/12)^2$  respectively, where the  $-q^2$  is shown in GeV unit using  $a^{-1} = 1.73(3)$  GeV [18]. Fitting range used for the mass estimate are  $6 \leq t \leq 23$  for pion and kaon or  $5 \leq t \leq 13$  for nucleon.

$(m_{ud}^{\text{sea}}, m_s^{\text{sea}})$	$m_{ud}^{\text{val}}$	$m_s^{\text{val}}$	$m_\pi$	$m_K$	$m_N$	$-q^2(\text{GeV}^2)$	# configs.	# meas.	
(0.005,0.04)	0.005		0.1897(5)		0.656(16)	-0.129	0.241	202	404
		0.005	0.0343		0.3131(5)	0.017	0.325		
		0.005	0.04		0.3322(5)	0.039	0.337		
(0.01,0.04)	0.01		0.2420(6)		0.705(16)	-0.162	0.194	150	150
		0.01	0.0343		0.3328(6)	-0.035	0.280		
		0.01	0.04		0.3510(6)	-0.011	0.295		
(0.02,0.04)	0.02		0.3228(6)		0.790(10)	-0.218	0.137	100	100
		0.02	0.0343		0.3681(6)	-0.142	0.189		
		0.02	0.04		0.3849(6)	-0.114	0.208		
(0.03,0.04)	0.03		0.3880(7)		0.912(11)	-0.391	-0.020	90	90
		0.03	0.0343		0.4003(6)	-0.364	-0.000		
		0.03	0.04		0.4160(6)	-0.330	0.025		

## B. Measurement of the form factor and kinematics

Figures 2 and 3 show the form factor  $W_0$  of the  $p \rightarrow \pi^0$  channel in Eqs. (26) and (27) as a function of the time position  $t$  of the three-quark operator. The open and filled symbols correspond to results in two different nucleon interpolating operators,  $(q^T C \gamma_5 q)q$  and  $(q^T C \gamma_4 \gamma_5 q)q$  respectively. To obtain the value of  $W_0$ , a simultaneous fit of these two effective  $W_0$  is performed at the plateau in the range  $13 \leq t \leq 20$ , where the two  $W_0$  appear to be consistent and the contamination from the excited states dies out. The same range is used for all the parameters and all the matrix elements. Figures 4 and 5 show  $W_0^{R/L}$  for each channel as a function of  $q^2$ .

The form factors in the physical kinematics are calculated from the extrapolation or interpolation with momentum and quark masses. For the physical kinematics of proton decay into meson and lepton final state,  $-q^2$  is equivalent to lepton mass squared in the relevant form factor  $W_0(q^2)$ . In the lattice computation, however, the quark masses are other parameters that need to be tuned toward the physical pion and kaon masses. Therefore we have three parameters to tune: degenerate  $u, d$  quark mass  $\tilde{m}_{ud}$ , strange quark mass  $\tilde{m}_s$  and meson momentum  $|\vec{p}|$ . In our simulation, the  $\tilde{m}_{ud} \rightarrow \tilde{m}_{ud}^{\text{phys}}$  limit is taken by an extrapolation,  $\tilde{m}_s \rightarrow \tilde{m}_s^{\text{phys}}$  limit is taken by an interpolation, where physical quark mass in lattice units is realized by the limit,

$$\tilde{m}_{ud}^{\text{phys}} = 0.001385, \quad (31)$$

$$\tilde{m}_s^{\text{phys}} = 0.03785, \quad (32)$$

with the values to reproduce the experimental hadron mass ratios,  $m_\pi/m_\Omega$  and  $m_K/m_\Omega$ , the pion and kaon mass over the mass of  $\Omega^-$  [18].

We employ two different procedures for taking the above limit. One is the global fit with a function that depends on both quark mass and  $q^2$ , and thus  $W_0$  at physical point is straightforwardly obtained. The other is to sequentially take the two limits; first  $q^2 \rightarrow 0$  and then take the quark mass to the physical point. In this procedure  $W_0$  at physical point is obtained by the second limit. In the next section we will show numerical results with these procedures.

### C. Extrapolation to physical kinematics with global fitting

In the global fitting to obtain the form factor in the physical kinematics we use the ansatz of linear function,

$$F_{W_0}^{\pi,\eta}(\tilde{m}_{ud}, q^2) = A_0 + A_1\tilde{m}_{ud} + A_2q^2, \quad (33)$$

$$F_{W_0}^K(\tilde{m}_{ud}, \tilde{m}_s, q^2) = B_0 + B_1\tilde{m}_{ud} + B_2\tilde{m}_s + B_3q^2, \quad (34)$$

with free parameters  $A_i$  and  $B_i$ .  $F_{W_0}^{\pi,\eta}$  is used for the pion or  $\eta$  final state,  $F_{W_0}^K$  for the kaon final state. This procedure is the same as that employed in the previous study [16]. We use four different quark masses, two different strange quark masses and the two lowest non-zero spacial momenta, and therefore the total number of data points is eight for  $\pi$  and

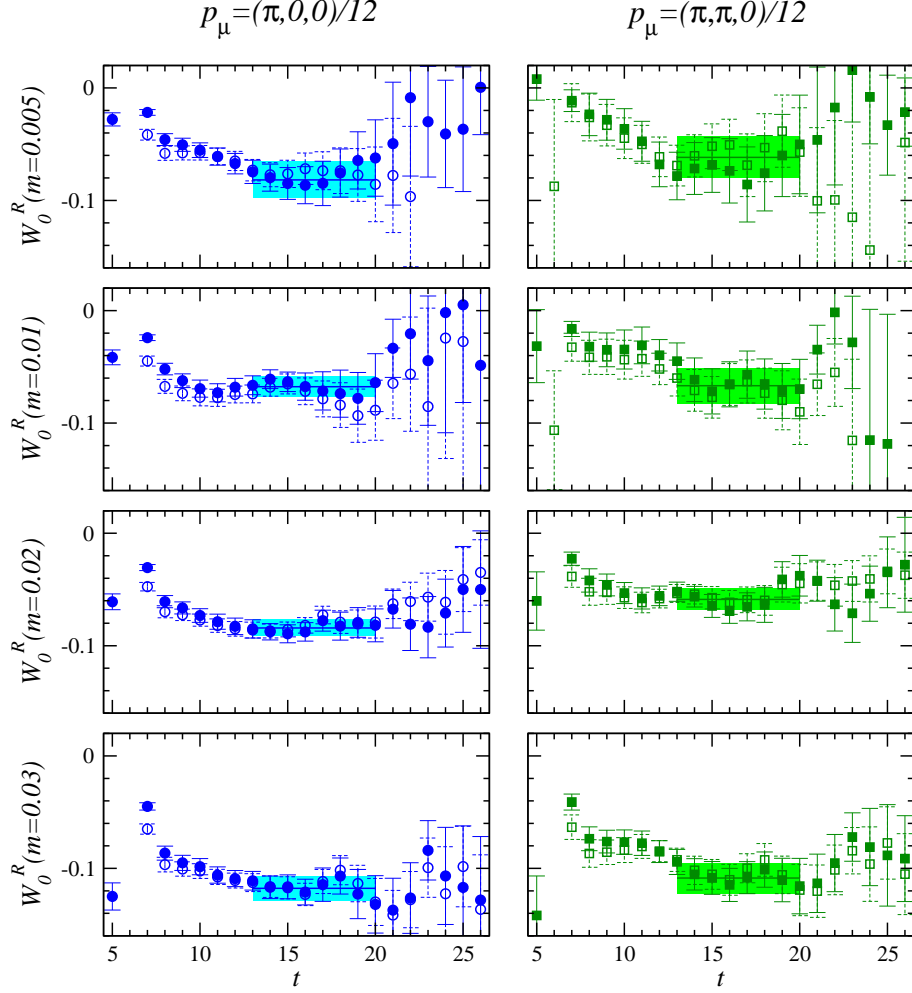


FIG. 2:  $W_0^R$  for  $p \rightarrow \pi^0$  decay channel is plotted as a function of operator time ( $t$  in Eq. (21)). The proton source is located at  $t = 5$ , and the  $\pi^0$  sink is at  $t = 27$ . Different symbols show the two different proton interpolating fields, which correspond to  $(u^T C \gamma_5 d)u$  (open) and  $(u^T C \gamma_4 \gamma_5 d)u$  (filled). The horizontal solid line indicates the central value of constant fit to the both plateaus in the range  $13 \leq t \leq 20$  simultaneously. The shaded area indicates 1-sigma error band.

$\eta$  or sixteen for the kaon final states. The results obtained with the global fit using all the data are shown in the second column in Table II. It turns out that the simple linear function as described in Eq.(33) and (34) is in good agreement with the lattice data for all channels, which is indicated by the reasonable  $\chi^2/\text{dof}$  ( $\leq 1.4$ ). The fit results  $F_{W_0}^{\pi;\eta}(\tilde{m}_{ud}^{\text{phys}}, q^2)$ ,  $F_{W_0}^K(\tilde{m}_{ud}^{\text{phys}}, \tilde{m}_s^{\text{phys}}, q^2)$  as a function of  $q^2$  at the physical masses are shown in Figs. 4 and 5.

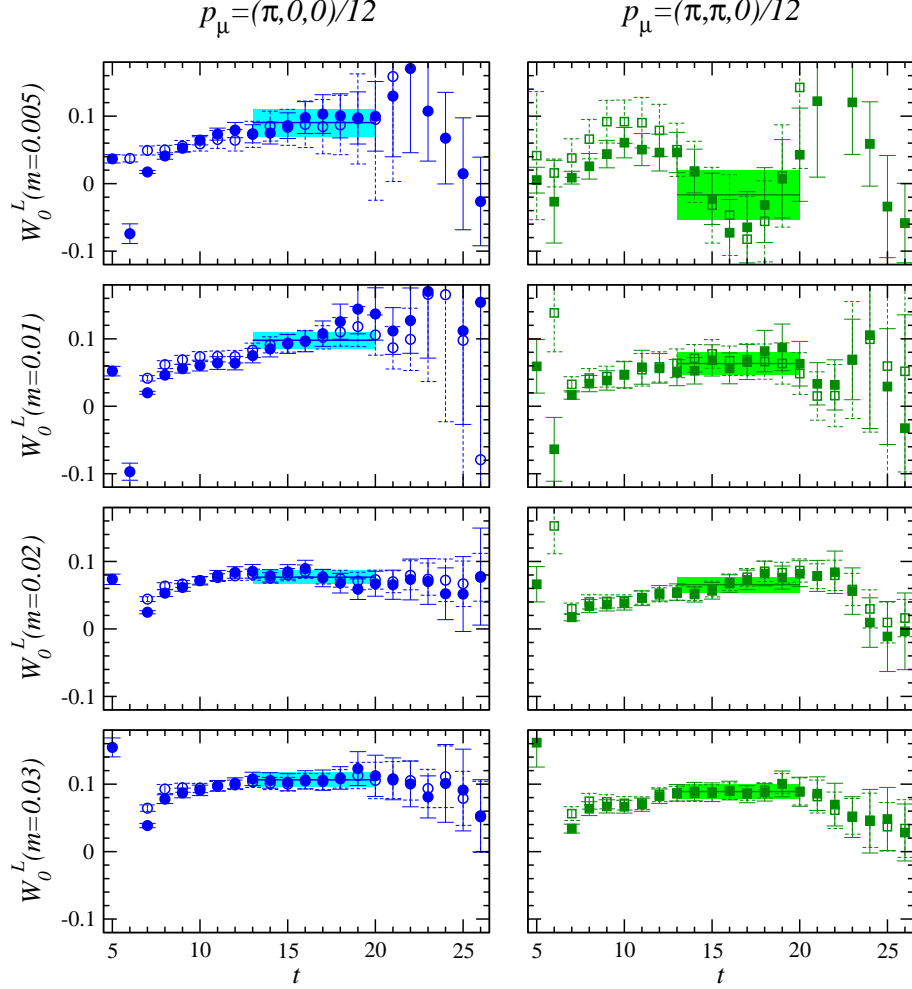


FIG. 3:  $W_0^L$  for  $p \rightarrow \pi^0$  decay channel is plotted as a function of operator time. Symbols are same as in Figure 2.

#### D. Extrapolation to physical kinematics with sequential fitting

In this procedure we first take the linear extrapolation or interpolation to  $q^2 = 0$  with two spatial momentum points in each mass  $\tilde{m}$  and then take a chiral extrapolation to physical quark mass. Figure 6 and 7 plot the results at  $q^2 = 0$  point as a function of  $\tilde{m}_{ud}$  after taking the  $q^2 = 0$  limit. In the chiral extrapolation of the fitted data at  $q^2 = 0$  we adopt the linear function as

$$f_{W_0}^{\pi,\eta}(\tilde{m}_{ud}) = a_0 + a_1\tilde{m}_{ud}, \quad (35)$$

$$f_{W_0}^K(\tilde{m}_{ud}, \tilde{m}_s) = b_0 + b_1\tilde{m}_{ud} + b_2\tilde{m}_s, \quad (36)$$

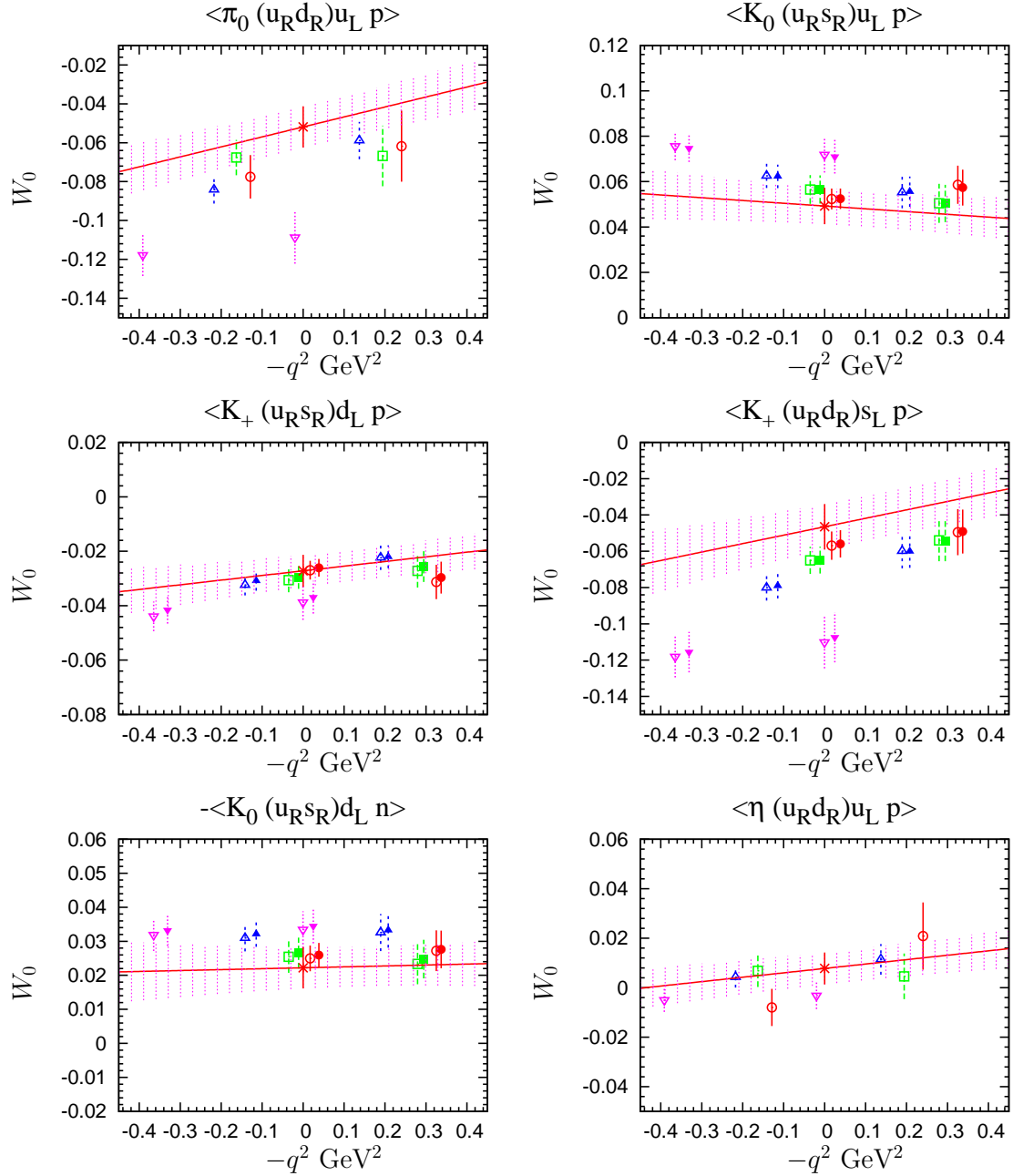


FIG. 4:  $q^2$  dependence of  $W_0^R(q^2)$  at all quark masses in lattice units. We plot the results at  $m_{ud} = 0.005$  (circle),  $m_{ud} = 0.01$  (square),  $m_{ud} = 0.02$  (up-triangle) and  $m_{ud} = 0.03$  (down-triangle). In the figure for  $K^{0,+}$ , results at  $m_s = 0.0343$  represent open symbol and filled symbol at  $m_s = 0.04$ . The solid lines (bands) show the global fit function (and its error) after taking the extrapolation into the physical quark mass using all of the points. The star symbol is the result at the physical kinematics using the global fit.

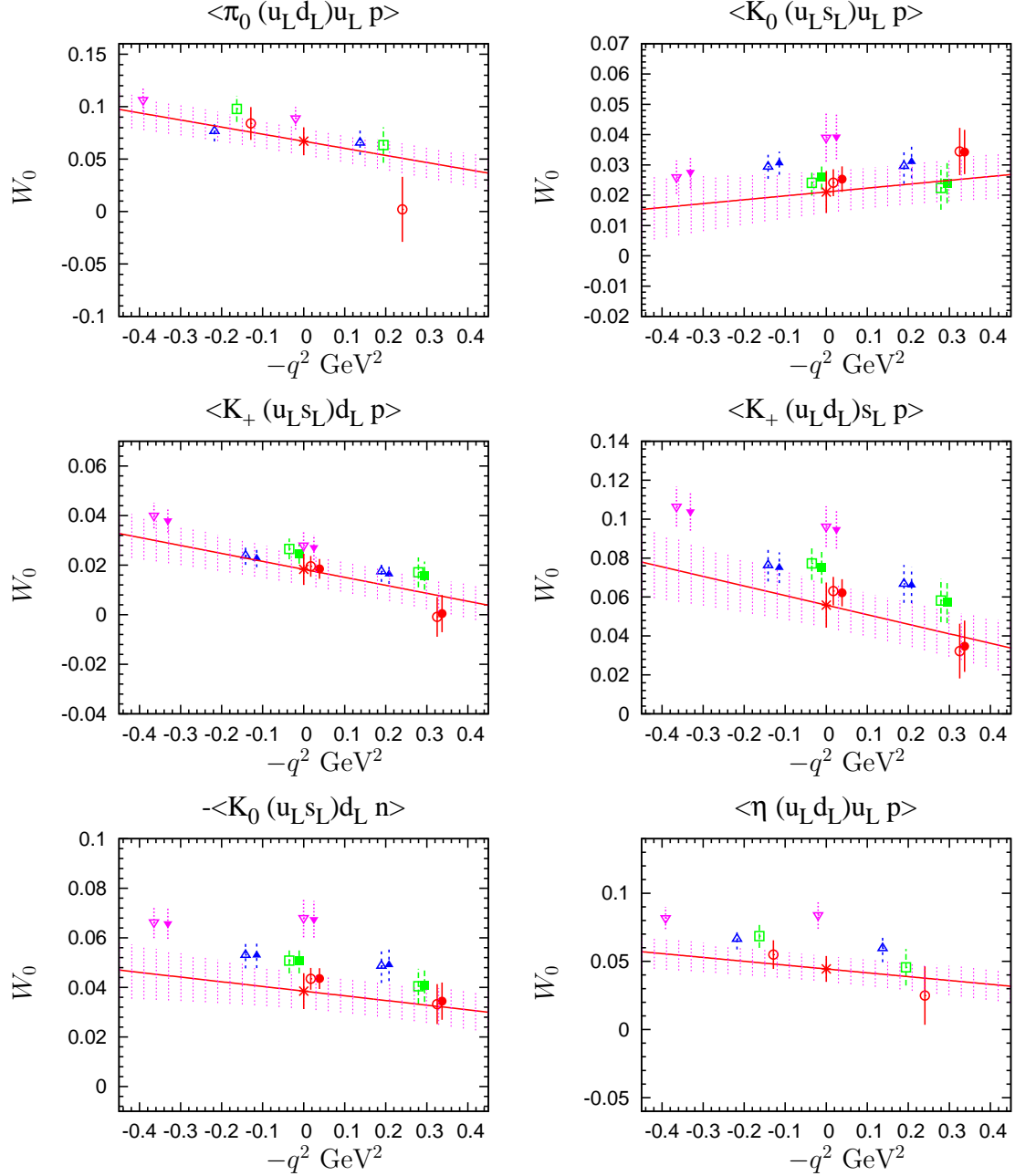


FIG. 5:  $q^2$  dependence of  $W_0^L(q^2)$  at all quark masses. Symbols are same as Figure 4.

for the pion,  $\eta$  final state or kaon final state respectively. Here  $a_i$  and  $b_i$  are the free fitting parameters. From Figure 6 and 7 we observe that the linear function describes the lattice results quite well for each matrix elements with four different mass points, except that the data for pion and eta in Fig. 6 seems to be less consistent with the linear ansatz. The difference of the four point fit and the three point fit will be used in the estimate of the

systematic error discussed later. The results are shown in Table II (see the column marked as “Sequential”).

### E. Systematic errors

The systematic errors due to using the extrapolation (or interpolation) into physical kinematics ( $q^2 = 0$  limit), contribution of finite volume and non-zero lattice spacing will be discussed in this section. This work uses the lattice scale estimated in Ref. [18] and the renormalization constant shown in Eq.(29) and Eq.(30). To estimate the total error apart from the statistical error, the systematic errors in the extrapolation, finite size effect and lattice artifact together with the error of lattice scale and of the non-perturbative renormalization procedure, are all added in quadrature.

At the target mass and momentum point  $(\tilde{m}_{ud}, \tilde{m}_s, q^2) = (\tilde{m}_{ud}^{\text{phys}}, \tilde{m}_s^{\text{phys}}, 0)$ , no chiral singularity is expected. Therefore, if the simulations are made closer to the target, the linear approximation to the fitting function becomes arbitrarily precise. However, as the simulated points might not be close enough to assume the linearity, we need to assess the systematic error due to the choice of this approximation. This systematic error is regarded as the effect of higher order than  $O(\tilde{m}_{ud})$  and  $O(q^2)$ . Note that the higher order effect beyond  $O(\tilde{m}_s)$  is safely neglected as its variation around the physical point is very small as can be estimated by comparing the results with  $m_s = 0.0343$  and  $0.04$  in Figs. 4 and 5.

The main results of the relevant form factors are employed as those by the global fit with  $0.005 \leq m_{ud} \leq 0.03$  (see in the second column of Table II). Note that  $r$  denotes the different fitting ranges

$$r_{\text{full}} : [0.005, 0.03], \quad r_{\text{heavy}} : [0.01, 0.03], \quad r_{\text{light}} : [0.005, 0.02] \quad (37)$$

which are also used in Table II. The variations of results removing the largest  $\tilde{m}_{ud}$  from the global fit, removing the smallest  $\tilde{m}_{ud}$  from the global fit and the result in sequential fit from the main result provide the systematic errors coming from uncertainty of the fitting function for the extrapolation to the physical kinematics and finite size effect (FSE).

The uncertainty in the extrapolation due to higher order effect than linearity in quark mass (and also  $q^2$ ) is estimated by variance between results in  $r_{\text{full}}$  and  $r_{\text{light}}$  and variance between results with global fit and sequential fit. By comparing the region with and without



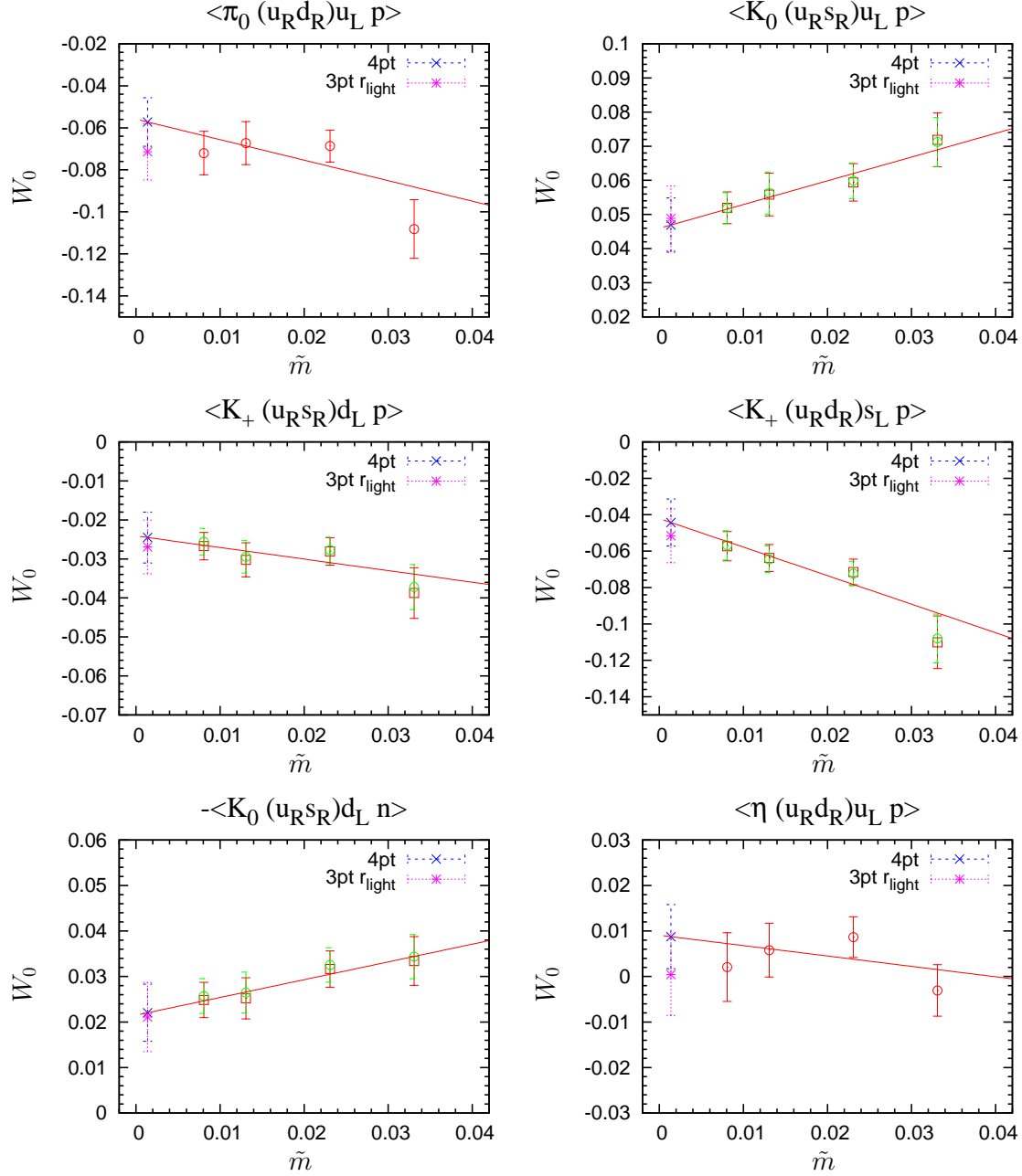


FIG. 6: Results of  $W_0^R(0)$  at different  $\tilde{m} = m_{ud} + m_{\text{res}}$ . The different open symbols shown in the matrix element of Kaon final state are the results at different partially quenched strange quark mass  $m_s = 0.0343$  (circle),  $m_s = 0.04$  (square). Straight lines show linearly fit function with all four quark masses. For the matrix element of  $p \rightarrow K$ , these are the results after taking the physical strange quark mass. The cross symbol is the result at physical light and strange mass with four fitting points and star symbol is with three fitting points using the range of  $r_{\text{light}}$  defined in the text. We discuss the systematic uncertainties by using the discrepancy between different fitting points (for example four fitting points and three fitting points) in Section IV E.

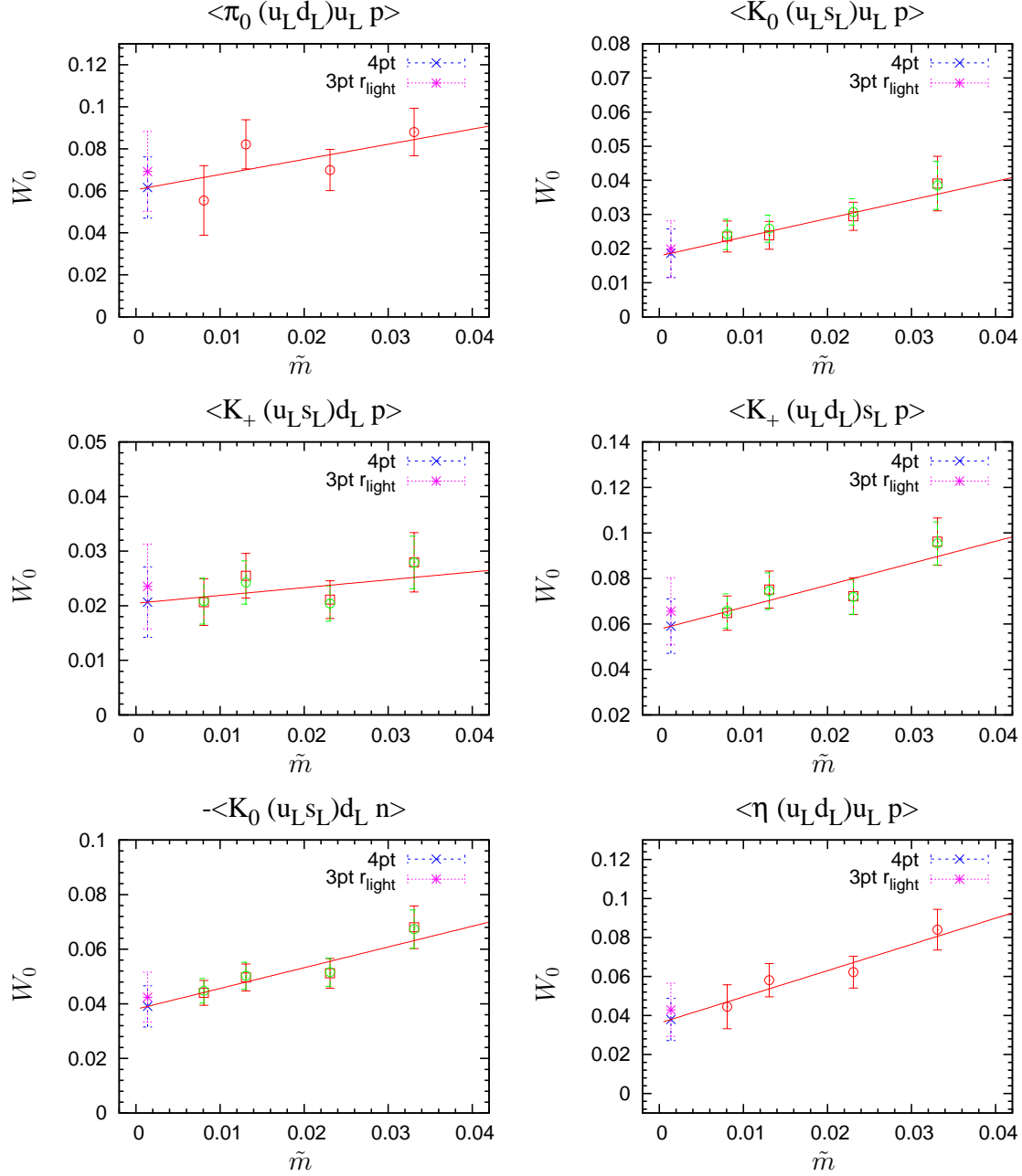


FIG. 7: Results of  $W_0^L(0)$  with same symbols as Fig.6.

heavy mass  $m = 0.03$  which is close to physical strange quark mass, we estimate the  $O(\tilde{m}^2)$  effect. Furthermore since sequential fitting procedure, explained in the previous subsection, takes into account the mass-dependence of  $q^2$  slope, we estimate the systematic error of the extrapolation to the physical kinematics as a part of the higher order effect, *e.g.*  $\mathcal{O}(\tilde{m}q^2)$  terms, beyond the  $\tilde{m}$  and  $q^2$  linear approximation by comparing with results in the global

fit.

On the other hand the difference between results in  $r_{\text{full}}$  and  $r_{\text{heavy}}$  is expected to probe at least a part of FSE since the lightest point is affected most from the FSE rather than  $O(\tilde{m}^2)$  effect. Such estimate of FSE has been known in the calculation of the nucleon axial charge  $g_A$  [24, 25] in which significant FSE was observed in the lightest quark mass in the same gauge ensemble. (This is also suggestive from the fact that the relevant form factor  $W_0$  for a pion final state is proportional to  $(1 + g_A)$  in the leading order of baryon chiral perturbation theory, see Ref. [16]). Therefore neglecting data at the lightest mass  $m = 0.005$  from the fitting region might include less contamination of FSE (see also Fig. 10 of Ref. [25]).

The systematic error including both higher order effect ( $O(\tilde{m}^2)$ ,  $O((q^2)^2)$ ,  $O(\tilde{m}q^2)$ ) and FSE is evaluated by adding in quadrature the difference between the global and sequential fitting results in the range of  $r_{\text{full}}$  and the maximum difference between global fitting results in the range of  $(r_{\text{full}}, r_{\text{light}})$  and  $(r_{\text{full}}, r_{\text{heavy}})$ , even though this procedure may be too conservative. The magnitude is shown in the column denoted as ‘‘Extrapolation’’ in Table III.

The discretization error of  $O(a)$  may arise from the inexact chiral symmetry due to finite  $L_s$ . However, as the size of the chiral symmetry breaking is small after the additive mass shift (Eq. 28) is performed:  $m_{\text{res}}a \simeq 3 \times 10^{-3}$ , this effect can be safely neglected. Here the dominant discretization error at  $O(a^2)$  has been estimated using the scaling study of hadronic observable performed with this and finer lattice ensembles [18]. The observed discrepancy in the spectroscopy of light meson (Fig. 26 in Ref. [18]) with the two lattice spacings is up to 1–2 %, which amounts to about 5% discretization error of the form factor  $W_0$  assuming the  $O(a^2)$  scaling. We take this 5% as the  $O(a^2)$  error, which is more conservative than a naive power counting  $(a\Lambda_{\text{QCD}})^2 \sim 0.02$  with  $\Lambda_{\text{QCD}} = 250$  MeV.

We also take into account the error coming from uncertainty of lattice spacing which is given in error of  $a^{-1} = 1.73(3)$  GeV and the error of the renormalization constant which is given in Eq.(29) or (30).

We ignore the partially quenched effect of strange quark, which is due to the small mismatch of the sea and valence strange masses, for the matrix element of  $K^+$ ,  $K^0$  meson final state. Since the valence strange quark mass dependence of  $W_0$  is negligibly small as shown in Fig.6 and Fig.7, this effect is also negligible. Note that we also do not consider the effect of disconnected diagrams in the matrix elements of the  $\eta$  in the final state, but

TABLE II: Table of results for renormalized  $W_0^{R/L}(\mu = 2\text{GeV})$  in  $\text{GeV}^2$  after global and sequential fitting. The error is only statistical one. For global fitting, we show the results with three different fitting mass-ranges, which are all in the range  $0.005 \leq m_{ud} \leq 0.03$  ( $r_{\text{full}}$ ), excluding the heaviest mass,  $m_{ud} = 0.03$ , ( $r_{\text{light}}$ ) and excluding the lightest mass,  $m_{ud} = 0.005$ , ( $r_{\text{heavy}}$ ). For the sequential fitting, we show the results including all the masses.

matrix element	Global				Sequential	
	$r_{\text{full}}$	$\chi^2/\text{dof}$	$r_{\text{light}}$	$r_{\text{heavy}}$	$r_{\text{full}}$	$\chi^2/\text{dof}$
$\langle \pi^0   (ud)_{RuL}   p \rangle$	-0.103(23)	1.4	-0.132(29)	-0.072(34)	-0.114(22)	2.2
$\langle \pi^0   (ud)_{LuL}   p \rangle$	0.133(29)	1.4	0.156(41)	0.142(38)	0.123(28)	1.1
$\langle K^0   (us)_{RuL}   p \rangle$	0.098(15)	0.4	0.103(19)	0.092(29)	0.093(15)	0.1
$\langle K^0   (us)_{LuL}   p \rangle$	0.042(13)	0.4	0.044(16)	0.037(20)	0.037(14)	0.1
$\langle K^+   (us)_{RdL}   p \rangle$	-0.054(11)	0.8	-0.060(13)	-0.052(21)	-0.049(13)	0.6
$\langle K^+   (us)_{LdL}   p \rangle$	0.036(12)	0.8	0.040(15)	0.041(18)	0.041(12)	0.6
$\langle K^+   (ud)_{RSL}   p \rangle$	-0.093(24)	0.6	-0.108(28)	-0.082(39)	-0.088(25)	0.9
$\langle K^+   (ud)_{LSL}   p \rangle$	0.111(22)	0.6	0.121(28)	0.115(37)	0.117(23)	0.7
$\langle K^+   (ds)_{RuL}   p \rangle$	-0.044(12)	0.1	-0.043(14)	-0.041(20)	-0.044(12)	0.1
$\langle K^+   (ds)_{LuL}   p \rangle$	-0.076(14)	0.3	-0.082(17)	-0.076(24)	-0.078(14)	0.5
$\langle \eta   (ud)_{RuL}   p \rangle$	0.015(14)	1.3	-0.002(19)	0.031(19)	0.017(14)	1.2
$\langle \eta   (ud)_{LuL}   p \rangle$	0.088(21)	0.7	0.094(29)	0.094(28)	0.076(21)	0.4

note that the result is valid assuming flavor SU(3) degenerate valence quark  $m_{ud}^{\text{val}} = m_s^{\text{val}}$  and ignoring partially quenched effect of the strange quark.

## F. Results of proton decay matrix elements

Table III summarizes the results of the relevant form factor  $W_0(q^2)$  of proton decay for all the principal matrix elements Eqs. (13), (15)-(19) at  $q^2 = 0$ . The central values are those obtained with the global fit on  $q^2$  and the simulated quark masses for the physical kinematics  $\tilde{m}_{ud} \rightarrow \tilde{m}_{ud}^{\text{phys}}$ ,  $\tilde{m}_s \rightarrow \tilde{m}_s^{\text{phys}}$  and  $q^2 \rightarrow 0$ , with the  $r_{\text{full}}$  range for  $m_{ud}$ . The values in the first parentheses are the statistical errors. The budget of systematic error is shown in the last

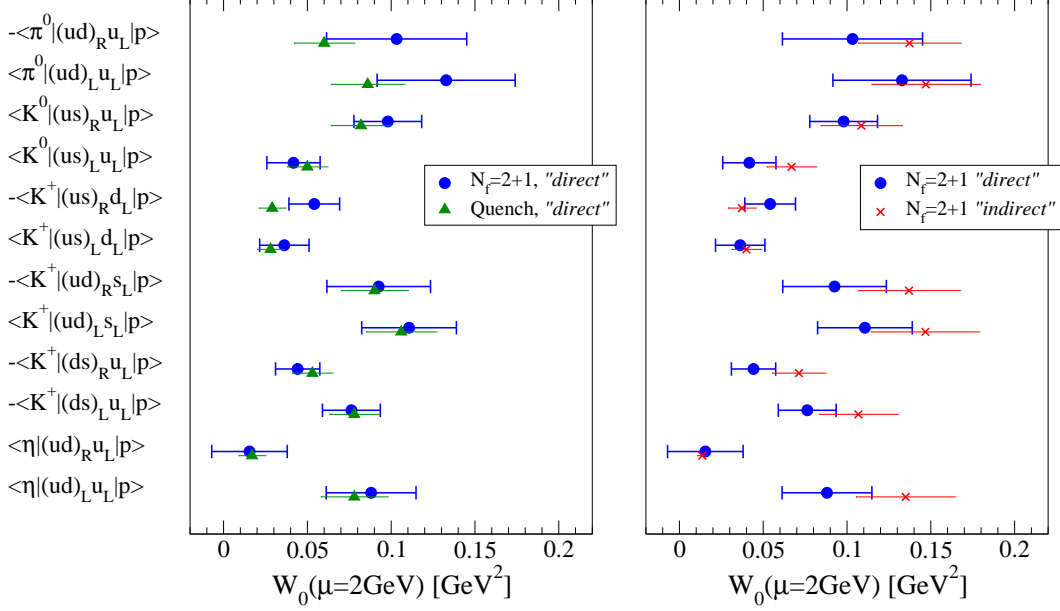


FIG. 8: Summary of  $W_0^{L/R}(\mu = 2\text{GeV})$  for twelve principal matrix elements. Filled circles show the present results, and for the comparison the results in quenched QCD (open circle) and *indirect* method using chiral perturbation theory (cross) are plotted in the same row.

four columns. These four errors are added in quadrature to give the total systematic error shown in the second parenthesis for each value of the form factor.

Figure 8 shows the results of the form factors with the error bars expressing the total error when statistical and systematic errors are added in quadrature, which are marked as “ $N_f = 2 + 1$ ”. The two panels compare the results with old ones using some approximation. The left panel compares against the results with quenched approximation in the *direct* method [16]. The right panel shows those with the *indirect* method in the same ensembles [17]. The sizable error for “ $N_f = 2 + 1$ ” in the current analysis prevents us from seeing any significant difference from the quenched or *indirect* results. For phenomenological applications, however, one should clearly use our  $N_f = 2 + 1$  results with the *direct* method with their total error instead of the previous results [16, 17], because each approximation previously has the systematic uncertainties which were not even estimated.

TABLE III: Final results of renormalized  $W_0^{L/R}(\mu = 2\text{GeV})$  for individual matrix elements and error budget of statistical and systematic uncertainties. The first and second errors in  $W_0^{L/R}$  represent statistical and systematic ones respectively. The third column denotes total error which is estimated by adding in quadrature statistical and systematic errors. The fourth column denoted as  $\chi$  shows the systematic error of mass and momentum extrapolation/interpolation estimated by the variance of extrapolation to physical kinematics and fifth column is uncertainties from lattice artifacts explained in the text. The last two columns show the uncertainties of renormalization factor ( $\Delta Z$ ) and lattice spacing ( $\Delta a^{-1}$ ). We also show the  $p \rightarrow \pi^+\bar{\nu}$  decay matrix element using SU(2) isospin relation in Eq.(20).

Matrix element	$W_0(\mu = 2\text{GeV})$	GeV <sup>2</sup>	Total error Systematic error budget				
			(%)	$\chi$	$\mathcal{O}(a^2)$	$\Delta Z$	$\Delta a^{-1}$
$\langle \pi^0   (ud)_{RuL}   p \rangle$	-0.103	(23) (34)	40	0.033	0.005	0.008	0.004
$\langle \pi^0   (ud)_{LuL}   p \rangle$	0.133	(29) (28)	30	0.026	0.007	0.011	0.005
$\langle \pi^+   (ud)_{RdL}   p \rangle$	-0.146	(33) (48)	40	0.047	0.007	0.011	0.006
$\langle \pi^+   (ud)_{LdL}   p \rangle$	0.188	(41) (40)	30	0.037	0.010	0.016	0.007
$\langle K^0   (us)_{RuL}   p \rangle$	0.098	(15) (12)	20	0.007	0.005	0.008	0.003
$\langle K^0   (us)_{LuL}   p \rangle$	0.042	(13) (8)	36	0.007	0.002	0.003	0.001
$\langle K^+   (us)_{RdL}   p \rangle$	-0.054	(11) (9)	26	0.008	0.003	0.004	0.002
$\langle K^+   (us)_{LdL}   p \rangle$	0.036	(12) (7)	39	0.007	0.002	0.003	0.001
$\langle K^+   (ud)_{RsL}   p \rangle$	-0.093	(24) (18)	32	0.016	0.005	0.008	0.003
$\langle K^+   (ud)_{LsL}   p \rangle$	0.111	(22) (16)	25	0.012	0.006	0.009	0.004
$\langle K^+   (ds)_{RuL}   p \rangle$	-0.044	(12) (5)	30	0.003	0.002	0.004	0.002
$\langle K^+   (ds)_{LuL}   p \rangle$	-0.076	(14) (9)	22	0.006	0.004	0.006	0.003
$\langle \eta   (ud)_{RuL}   p \rangle$	0.015	(14) (17)	147	0.017	0.001	0.001	0.001
$\langle \eta   (ud)_{LuL}   p \rangle$	0.088	(21) (16)	30	0.014	0.004	0.007	0.003

## V. SUMMARY AND OUTLOOK

We have presented the lattice calculation of proton decay matrix elements using 2+1 flavor dynamical domain-wall fermions, which are essential ingredients to estimate the nucleon lifetime in grand unified theories. The *direct* method using three-point function (nucleon)-

(operator)-(meson), with non-perturbative renormalization, was applied on a volume  $L_\sigma^3 \simeq 3 \text{ fm}^3$ . Previous calculations had undermined estimate of systematic uncertainties on the matrix elements at the physical kinematics. This work made it possible to control these uncertainties for the first time, by removing most of them, while remaining uncertainties were given with their estimates. The uncertainties that have been eliminated here are those due to the quenched approximation [16] and the use [17] of the *indirect* method with the tree-level baryon chiral perturbation theory. The estimated uncertainties are the error in the extrapolation in quark mass and meson momentum, finite volume effect, discretization error, error in the non-perturbative renormalization and the uncertainty of the lattice scale. The relevant form factors  $W_0(q^2 = 0)$  of the twelve principal matrix elements Eqs. (13), (15)-(19), from which one can calculate those for all the nucleon to pseudoscalar meson process, has been evaluated and summarized in Table III with their error estimates.

Although we have established an estimate of the proton decay matrix element with all the errors, the total errors are fairly large (30%–40% for  $\pi$  final state and 20%–40% for the  $K$  final state). One of the major uncertainty is the statistical error, especially for  $p \rightarrow e^+\pi^0$  decay mode, and that could have influenced the size of the error of combined chiral extrapolation and finite volume effect. A significant improvement of the current results is expected by adopting the newly developed technique for reduction of the statistical error [26], which will be addressed in future work. We want to emphasize, though, for now in any serious phenomenological application one should use the results in this study with the stated total errors.

## Acknowledgments

We thank the members of RBC/UKQCD collaborations for their valuable help with comments and encouragement. We especially would like to thank Peter Boyle, Paul Cooney, Chris Dawson, Luigi Del Debbio, Taku Izubuchi, Chulwoo Jung, Adam Lichtle, Chris Maynard, Robert Tweedie. Numerical calculations were performed on QCDOC computers of USQCD collaboration and RIKEN BNL Research Center for which we thank US DOE and RIKEN BNL Research Center. A. S. is supported by U.S. DOE contract DE-AC02-98CH10886. This work is also supported, in part, by JSPS Kakenhi Grant Nos. 21540289,

22224003 (YA), and by MEXT Kakenhi Grant Nos. 23105714 (ES) .

---

- [1] J. C. Pati and A. Salam, Phys. Rev. Lett. **31**, 661 (1973).
- [2] H. Georgi and S. L. Glashow, Phys. Rev. Lett. **32**, 438 (1974).
- [3] J. Hisano, H. Murayama, and T. Yanagida, Nucl. Phys. **B402**, 46 (1993), hep-ph/9207279.
- [4] H. Murayama and A. Pierce, Phys. Rev. **D65**, 055009 (2002), hep-ph/0108104.
- [5] H. Nishino et al. (Super-Kamiokande), Phys.Rev.Lett. **102**, 141801 (2009), 0903.0676.
- [6] H. Nishino et al. (Super-Kamiokande), Phys.Rev. **D85**, 112001 (2012), 1203.4030.
- [7] K. Kobayashi et al. (Super-Kamiokande), Phys. Rev. **D72**, 052007 (2005), hep-ex/0502026.
- [8] C. Regis et al. (Super-Kamiokande Collaboration) (2012), 1205.6538.
- [9] P. Nath and P. Fileviez Perez, Phys. Rept. **441**, 191 (2007), hep-ph/0601023.
- [10] K. Abe, T. Abe, H. Aihara, Y. Fukuda, Y. Hayato, et al. (2011), 1109.3262.
- [11] Y. Hara, S. Itoh, Y. Iwasaki, and T. Yoshie, Phys. Rev. **D34**, 3399 (1986).
- [12] K. C. Bowler, D. Daniel, T. D. Kieu, D. G. Richards, and C. J. Scott, Nucl. Phys. **B296**, 431 (1988).
- [13] M. B. Gavela et al., Nucl. Phys. **B312**, 269 (1989).
- [14] S. Aoki et al. (JLQCD), Phys. Rev. **D62**, 014506 (2000), hep-lat/9911026.
- [15] N. Tsutsui et al. (CP-PACS), Phys. Rev. **D70**, 111501 (2004), hep-lat/0402026.
- [16] Y. Aoki, C. Dawson, J. Noaki, and A. Soni, Phys. Rev. **D75**, 014507 (2007), hep-lat/0607002.
- [17] Y. Aoki et al. (RBC and UKQCD), Phys. Rev. **D78**, 054505 (2008), 0806.1031.
- [18] Y. Aoki et al. (RBC and UKQCD), Phys.Rev. **D83**, 074508 (2011), 1011.0892.
- [19] S. Weinberg, Phys. Rev. Lett. **43**, 1566 (1979).
- [20] F. Wilczek and A. Zee, Phys. Rev. Lett. **43**, 1571 (1979).
- [21] L. F. Abbott and M. B. Wise, Phys. Rev. **D22**, 2208 (1980).
- [22] C. Alexandrou, S. Gusken, F. Jegerlehner, K. Schilling, and R. Sommer, Nucl.Phys. **B414**, 815 (1994), hep-lat/9211042.
- [23] M. Lin et al. (RBC and UKQCD), PoS **Lattice 2012**, 172 (2012).
- [24] T. Yamazaki et al. (RBC and UKQCD), Phys. Rev. Lett. **100**, 171602 (2008), 0801.4016.
- [25] T. Yamazaki et al., Phys. Rev. **D79**, 114505 (2009), 0904.2039.
- [26] T. Blum, T. Izubuchi, and E. Shintani (2012), 1208.4349.